Title: Adaptation to Full-field Contrast Encoding in Distinct Layers of Macaque Primary Visual Cortex

Abbreviated title: Laminar contrast encoding in V1

Lazaros Mitskopoulos[1], Sangkyun Lee[2,3], Wangchen Wang, Andreas S. Tolias[4], Maria Papadopouli[5,6], Ioannis Smyrnakis[6] and Stelios Manolis Smirnakis[2,3]

[1] School of Informatics, University of Edinburgh, 10 Crichton Street, Edinburgh EH8 9AB, UK

[2] Department of Neurology, Brigham and Women's Hospital, Boston, MA, 02115 United States

[3] Boston VA Research Institute, Jamaica Plain Veterans Administration Hospital, Harvard Medical School, Boston, United States

[4] Department of Neuroscience, Baylor College of Medicine, Houston, TX, United States

[5] Department of Computer Science, University of Crete, Heraklion,70013, Greece

[6] Institute of Computer Science, Foundation for Research and Technology Hellas (FORTH), Heraklion, 70013, Greece

Corresponding author: Stelios M Smirnakis smsmirnakis@bwh.harvard.edu

Number of pages: ???

Number of figures and multimedia: ???

Number of words for Abstract, Introduction, and Discussion: 251, ?, ?

Conflict of interest: The authors declare no competing financial interests

Acknowledgements: This work has been funded from the Hellenic Foundation for Research and Innovation (HFRI) and the General Secretariat for Research and Technology (GSRT) under grant agreement No 2285, as well as by NEI RO1 R01 EY019272 to SS.

Abstract: The neocortex is composed of six main layers of neurons that form an intricate microcircuit with connections within a cortical area and the rest of the brain (Callaway, 1998). This laminar circuit motif has been proposed to be the fundamental module of cortical computational processes (Mountcastle, 1978; Douglas and Martin, 2010). However, the algorithmic principles as well as the functional role of each layer remain unclear to date. In this study, we conducted a systematic investigation of the information coding properties for stimulus contrast across different cortical layers of the macaque primary visual cortex. We adopted an approach using a uniform-field flicker stimulus with alternating contrast conditions and analyzed the statistical features of the distribution of stimuli that elicited spikes (Smirnakis et al. 1997; Meister and Berry, 1999; Liu and Gollisch, 2015) as a function of time after the transition. Neural responses were modelled as linear-nonlinear (LN) functions (Schwartz et al., 2006), whose linear component was taken to be proportional to the neurons' spike-triggered average (STA) responses. We found that both the parameters of the STA and the nonlinearity during the steady-state contrast response varied systematically both between contrast levels and across cortical depths. Closer investigation of the dynamics of adaptation to new contrast conditions revealed a rich repertoire of trajectories for the firing rate, the STA and the nonlinearity.

1 Introduction

The visual sensory system constantly receives stimuli whose statistics can vary considerably across multiple spatial and temporal scales. If the brain operates as an efficient encoder (Barlow et al., 1961), visual neurons have to represent deviations from a mean luminance level such that the range of contrasts matches the dynamic range of spiking responses (Laughlin, 1981). Adaptation to contrast can potentially affect a cell's computational properties while inducing changes in feature tuning or its response sensitivity(Solomon and Kohn, 2014). In the mammalian primary visual cortex, a considerable number of studies have investigated contrast-related effects in single neuron responses. Although many neurons tend to increase their activity at high contrasts until a saturation point, some key properties of their receptive fields such as orientation, direction and spatial frequency selectivity appear to be contrast invariant (Chao-Yi and Creutzfeldt, 1984; Skottun et al., 1987; Anderson et al., 2000; Albrecht et al., 1984; Sclar and Freeman, 1982; Albrecht, 1995; Albrecht and Geisler, 1991; Van Hooser et al., 2005; Nowak and Barone, 2009). These observations were proposed to result from contrast gain control,

which maintains neuronal feature coding by reducing the sensitivity of cells to stimulus fluctuations in high contrasts (Shapley and Victor, 1978; Ohzawa et al., 1982; Albrecht et al., 1984; Ohzawa et al., 1985; Sclar et al., 1989). Such adaptive changes take place at all stages of the visual hierarchy and have several components that occur on a multiplicity of time scales (reviewed in Wark et al, 2007 and Weber et al, 2019). In general, adjustments that relate to feature tuning have been shown to happen within less than 100 ms after a change in contrast in the retina (Victor, 1987; Chander and Chichilnisky, 2001; Baccus and Meister, 2002)(but see Smirnakis et al, 1997) as well as the visual cortex (Sharpee et al., 2006; Ghodrati et al., 2019). However, adaptive changes related to contrast sensitivity and spiking frequency can unfold over several seconds or minutes (Ohzawa et al., 1985; Smirnakis et al., 1997; Baccus and Meister, 2002; Sharpee et al., 2006; Ghodrati et al., 2019) ,(see Wark et al, 2007 for a review). The underlying mechanisms as well as the functional role of these various components are still not fully understood but it is very likely that they arise from a combination of intrinsic single-cell mechanisms such as synaptic depression (Chance et al., 1998; Carandini et al., 2002) and circuit ones such as divisive normalization (Heeger, 1992; Carandini et al., 1999; reviewed in Weber et al, 2019).

While a number of studies has focused on single cell mechanisms (reviewed in Solomon and Khan, 2014), it remains largely unknown how contrast adaptation manifests in the cortical microcircuit. Disentangling potential intracortical interactions requires a detailed analysis of laminar processing of image contrast, which is absent in the literature. Past research on the lamination of neuronal functional properties in V1 have had mixed results. Although some studies reported differences in spontaneous firing rates, noise correlations, response-onset latency and feature tuning ((Snodderly and Gur, 1995); Hawken et al, 1996; (Schmolesky et al., 1998); (Self et al., 2013)), others found no laminar or cell type (simple vs complex) dependence for contrast adaptation speed and temporal frequency tuning (Ohzawa et al, 1985; Hawken et al, 1996). Therefore, it is not clear what the role of layers in contrast adaptation is or whether they play any important role at all.

Our study aimed to shed light into the aforementioned issues by conducting a detailed analysis of contrast adaptation across the cortical layers in macaque primary visual cortex. To that end, we employed a simplified stimulation protocol, namely a uniform-field flicker stimulus, previously used in studies in the retina (Smirnakis et al, 1997; Liu and Gollisch, 2015). We modelled temporal contrast encoding with single neuron linear-nonlinear (LN) models (Schwartz et al, 2006) to describe both feature tuning (linear filter) and response sensitivity(nonlinear response function). We hereby show that contrast-

induced changes in cell responses and LN descriptions challenge the notion of invariance. Moreover, these changes appear to share both similar and different features across the cortical layers.

2 Materials and Methods

2.1 Data collection

The data were collected from the primary visual cortices of 3 anesthetized adult rhesus macaques using chronically implanted 24-tetrode arrays. These are the same animals from Ecker and collaborators (2014), where details regarding the surgical procedure and the electrophysiological recordings are fully described. Neuronal activity was recorded at a 30 kHz sampling rate for each recording site, and the tetrode arrays were subsequently advanced by approximately 100-150 μm in increasing depths through the cortical layers. Action potentials were detected offline when the amplitude of the signal from any of the four channels was five times larger than the standard deviation on the corresponding channel. Spike sorting was performed for action potentials recorded in the same site, utilizing methods that were developed by Tolias et al (2007; Ecker et al, 2014). In brief, the principal components of spike waveforms were extracted and the resulting features were used for clustering to reveal putative single cells. The clusters were fitted with a mixture of Gaussians model, which was also used to estimate cross-contamination/overlap between clusters. Quality of single-unit isolation was, thus, assessed by considering the aggregate percentages of false positives and false negatives in cluster assignments. The former referred to the spikes that were assigned to a particular cluster but were generated by another while the latter referred to spikes that were generated by a cluster but assigned to another. We excluded from the analysis the set of all cells with composite false positive and false negative rate beyond 10 % of the total spikes. Moreover, as an additional criterion for the quality of isolation, we considered the percentages of refractory period violating (under 2ms) inter-spike intervals per cell. The set of cells that contained more than 5 % of such intervals were also excluded from the analysis. While we ensured the isolation quality of the cells for analysis, it is important to note that any possible cross-contamination is present only among cells of the same tetrode and not between different recording sites or different depths.

2.2 Stimulation

The cells were stimulated with spatially uniform grayscale luminance that changed every 2/60 seconds and each value was drawn randomly from a Gaussian distribution (Figure 1.A). The stimulation alternated between low and high contrast ensembles (Figure 1.B) that had the same mean luminance (i.e. 127.5/255 in the photopic range) but different standard deviations, namely, $\sigma = 6/255$ for low and $\sigma = 35/255$ for high contrast. An entire stimulation session consisted of 30 repetitions of 60-sec long blocks for each contrast level, presented in alternating sequence (Figure 1.B).

2.3 Depth classification

We grouped the recording sites into three major categories of depth according to the laminar domain where they were situated, namely granular, supragranular and infragranular (Balaram et al, 2014). The classification was based on the Current-Source Density (CSD) temporal trace across the depth of V1 (Mitzdorf, 1985).For CSD analysis, a spatially uniform stimulus with the maximum luminance was presented for 1 second, which was followed by 4 seconds of presentation of the mean luminance gray screen.This stimulation was repeated 50 times in each depth session and this experiment was performed across all depth sessions prior to the main experiment. The CSD analysis was performed by analyzing local field potentials in response to the stimulus within each tetrode site. The signal was first lowpass and highpass filtered to have a frequency range of 1 to 100Hz. Then, the visually evoked responses to the stimulus were aligned with respect to the relative stimulus onset time across depths and were treated as simultaneously recorded. To consider irregular sampling in depth,a kernel CSD method was applied (Potworowski et al. 2012).

We identified the granular layer (layer 4) as the spatial region that exhibited the deepest current sink within a temporal window of 50-150 ms after a pulse stimulation. The regions above and below the granular layer were characterized by the presence of transient current sources at distinct phases within the same temporal window. The recording sites located at these regions were classified accordingly as supragranular (layers 2/3) and infragranular (layers 5 and 6) V1 layers. Lastly, a number of sites that were between source and sink areas were defined as border regions either between granular and supragranular or granular and infragranular layers [CSD stimulation and analysis to be filled in here].

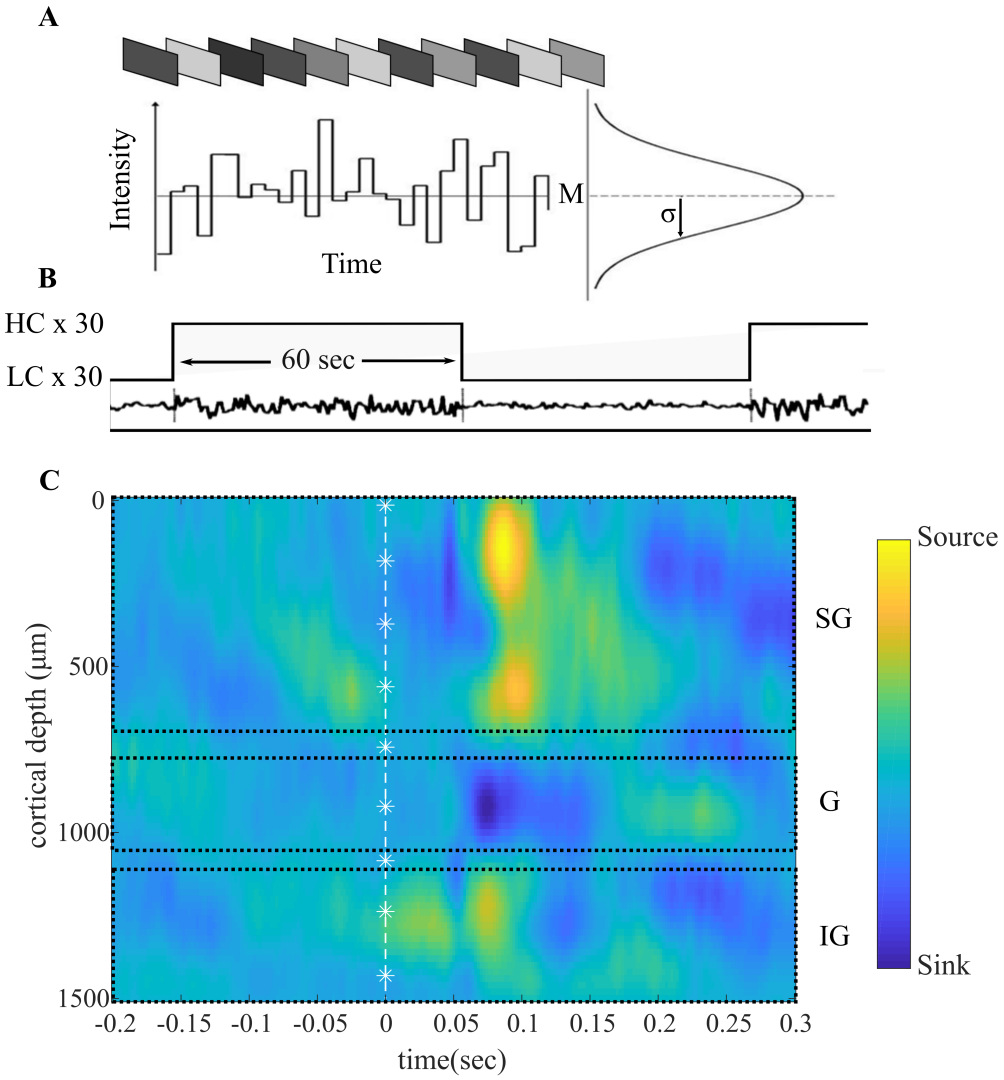

Figure 1: Stimulation protocol and Current Source Density (CSD) analysis **A.** Shaded rectangles on top depict the spatially uniform screen at different intensities. The light intensity was piecewise constant for 33.3 ms and changed abruptly to the next value which was randomly drawn from a Gaussian distribution (second row). The mean luminance M, was the same but the standard deviation σ changed periodically to a wide or short range of light intensities. **B.** The entire stimulation period consisted of thirty cycles of low (LC) vs high contrast (HC) 60-sec long stimulus epochs, for a total of 1 hour. **C.** CSD profile plotted as a function of cortical depth in μm and time in seconds relative to the maximum luminance stimulus onset ($t = 0$, white dashed line). Current is color-coded on a scale from negative (sink) to positive (source) values. Tetrode recording sites (white asterisks) that were located in regions enclosed with dashed rectangles were assigned to the supragranular (SG), granular (G) or infragranular (IG) domain. Non-enclosed regions between sinks and sources were considered as border regions.

2.4 Firing rate adaptation

In order to assess the stationarity of neural responses, we calculated the mean firing rate of each clustered unit/putative cell in each tetrode and depth, over the whole course of the recording session. We determined whether a neuron's spike train contained non-stationary segments with the following procedure. We estimated the temporal averages and standard deviations in the first two stimulus blocks. Then, if any subsequent block exhibited firing rate that exceeded twice the standard deviation of the temporal averages, that particular block was marked as non-stationary and was not considered in the analysis.

We then sought to identify all contrast-responsive cells, that is the ones with significantly different responses after an upward and a downward step in contrast. Given that adaptation could either take place almost immediately or gradually over several seconds (Ozhawa et al, 1985; Smirnakis et al, 1997; Baccus and Meister, 2002; Sharpee et al, 2006; Ghodrati et al, 2019), significant changes in activity could be observed either at the early phase (first 6 secs) or at steady state (48-60 seconds). Therefore, we applied Wilcoxon rank-sum tests that compared the steady state block-averaged activity in low contrast with both the early and the steady-state block-averaged activity in high contrast. In order to describe the time course of slow adaptation, we fitted the block-averaged activity trajectories (Figure 2.A) with exponential models of the form:

$$r(t) = a + b(e^{\frac{t}{\tau}}) \tag{1}$$

where a, b and τ are free parameters, and τ is the time constant that quantifies the rate of exponential adaptation. We evaluated the significance of the fitted models with ANOVA tests. For the significant fits, we extracted the features of the exponential model that characterize the adaptation, namely the initial firing rate at the first time point after contrast transition, the steady state rate at the last time point of the block, and the adaptation constant, τ.

2.5 Linear-nonlinear characterization of contrast responses

We characterized each neuron's response to the uniform-field flicker by a linear-nonlinear model (Schwartz et al, 2006). In this formulation, the firing rate, *r(t)*, is determined by a weighted sum of a sequence of preceding inputs, *s(t)*, which is passed on to a nonlinear function, *f*.

$$r(t) = f(\sum ws(t)) \tag{2}$$

This characterization corresponds to the estimation of a temporal linear filter w and the nonlinear function f. Our aim was to investigate encoding differences across the cortical layers by assessing whether the parameters of the linear and the nonlinear model components varied significantly with respect to cortical depth.

We restricted the first stage of this analysis to the steady-state part of the spiking responses, i.e. after each cell had adapted to the transition of contrast level. The length of the adaptive stage varies considerably among neurons in V1 as demonstrated both in past studies (Ohzawa et al, 1982, 1985; Sharpee et al, 2006; Levy et al, 2013) as well as in our data. We could not rely on individual time-constants to determine the adaptive stage as not all neurons could be fit with an exponential model, and even among those that could, the highly variant time-scale of adaptation would result in a massively uneven exclusion of spike train segments for different neurons. Thus, we chose the median time-constant for all cells per contrast to determine a common starting point for the steady state.

At the second stage of this analysis, we sought to answer whether the features of the linear and nonlinear components adapted immediately or gradually after changes in contrast. Instead of excluding the adaptive stage, we divided the block duration in 10 consecutive 6-second bins, with the first bin starting immediately after each contrast transition and the last bin ending at the 60 seconds, i.e. the end of each block.

2.5.1 Spike-Triggered Average

Provided that the stimulus distribution is Gaussian, a single linear filter can directly be estimated with the spike-triggered average (STA), i.e. the average deviation from the stimulus mean that preceded a spike. We calculated the STA separately for low and high contrast stimuli, for every cell in each tetrode and cortical depth, according to the following formula (Aljadeff et al, 2016):

$$STA = \frac{1}{N}\sum_{i=1}^{N} n(t_0)_i s(t)_i \tag{3}$$

For each spike a neuron emitted, we selected the preceding stimulus values *s(t)*, in a temporal window

t of millisecond resolution, which included an entire second before the spike. Each *s(t)* sequence in the sum was mean centered, divided by the standard deviation of its luminance distribution and multiplied by the number of spikes $n(t_0)$ that occurred at time t_0, the most recent time-bin of the window t, and the entire sequence ensemble was averaged over the total number of spikes, N. In addition to the spike-triggering stimuli, we also selected an equal sample of stimulus values within the second immediately after each spike. Because neurons are causal, these advanced stimuli had no influence on the spike that they followed and thus formed a control ensemble.

To assess whether the deviations in the STA waveforms are significantly different than random fluctuations, we measured the ratio of the amplitude of the most prominent peak for each STA over the standard error of the mean (SEM), at the time point of that peak, separately for low and high contrast. We also extracted an equivalent ratio from the point of maximum amplitude in the advanced STA. Subsequently, we subtracted the ratios of the advanced STAs from the ones of the pre-spike STAs and the resulting quantity was considered as a criterion for determining significant STA peaks. Any peak with a ratio that was greater than 3 was deemed significant. Only the STAs that had at least one significant peak were considered in the analyses. Moreover, we relied on this criterion to identify different types of STAs based on the number of the peaks found to be significant.

To obtain a signature of the STAs that enables comparisons across cortical depths, we extracted a set of time-domain parameters pertaining to the peaks of each STA. More specifically, for each significant primary and secondary peak, we measured their time to peak before the spike, their width at half-amplitude, their amplitude and their peak-to-peak amplitude (Figure 4.A points of interest a, b, c and d respectively). The peak order from the first to the last was defined according to the proximity to the spike, with the first being the most proximal. Furthermore, we also extracted the length of the STA temporal integration window (Figure 4.C e) which we employed for computing the response function. To estimate the length of this window we identified the peak that was most distal to the spike and moved by a step twice its width at half amplitude towards the tail of the waveform.

The criteria and parametrization that we conducted at the steady-state analysis were the same for the second stage analysis which tracked the adaptation dynamics of the STA.

2.5.2 Effective stimulus response function

Although the STA represents a cell's first-order feature tuning, it does not provide the full picture of the neuronal response, which requires an additional estimation of the nonlinearity f, denoted in (2). To estimate the nonlinearities for every neuron at steady-state, we computed the effective stimulus response functions, separately in low and high contrast, for each neuron that yielded significant STAs. We obtained the effective stimulus by a sliding projection of the entire input stimulus separately for low and high contrast onto the neuron's STA, with a step-size of 2 ms. The same procedure and subsequent analysis was followed for tracking the adaptation dynamics of the response function, albeit separately for each 6-second segment of the blocks. The effective stimulus distributions in both contrasts were transformed in units of standard deviation of the low contrast distribution. The firing rate predictions across the distribution were calculated by dividing the spike counts we found within 2 ms after each effective stimulus value, with the aggregate time from all 2-ms bins after each such value occured.

We characterized the response function of each neuron by fitting the firing rate predictions with sigmoid models. Since cortical nonlinearities can assume various shapes (Rust et al, 2004) we employed either single sigmoid models for the entire effective stimulus range, or a combination of such models separately for the positive and the negative semi-axes. Each nonlinearity was parametrized by its slope, its threshold and its upper and lower plateaus (Figure 6.B). The slope was defined as that of the tangent line at the half of the maximum modulation. Since the dynamic range could vary considerably in different cells we normalized the response curves with respect to the maximum firing rate prediction in each cell, prior to the slope extraction. The effective threshold was defined as the x-axis intercept of the tangent at the half-maximum. This threshold signified an estimate of the point in the effective stimulus where the firing rate modulation took off exponentially. Finally, the maximum and minimum predicted firing rates were extracted from the upper and lower sigmoid plateaus, respectively.

3 Results

In order to investigate how different layers in the primary visual cortex encode stimuli of different contrasts, we analyzed the responses of cells recorded from 3 anesthetized rhesus macaques. The total number of the recorded putative cells was 590, 854 and 929 for the first, second and third subject, respectively. Out of this sample, we found that a combined subset of 1536 were well-isolated cells,

that is below the contamination threshold we defined (see Materials and Methods: Data collection). The laminar domains for the sites of these well-isolated cells were determined from the CSD analysis. The 255 cells (16.7%) who were located in the current sink were labelled as granular while 680 cells (44.2%) at the sink reversal from above and 264 cells (17.1%) at the deeper sink reversal were labelled as supragranular and infragranular respectively. The remaining 337 cells (22%) were located between source and sink regions, and thus were considered as border-zone due to the uncertainty regarding the depth assignment. Although these 1199 cells comprised the sample for all our analyses, every subsequent stage involved further exclusion criteria.

3.1 Firing rate adaptation

The majority of the recorded V1 cells modulated their firing rate following contrast switches, but responses varied within the population and between cortical layers. We identified 726 contrast-responsive cells with significantly different mean activity either in the first time bin, i.e. during the first 6 seconds (see Materials and Methods: Firing rate adaptation) after a change in contrast or at steady state, i.e. at 48-60 seconds after contrast change(Wilcoxon rank-sum test, $p < 0.05$). Following previous studies (Smirnakis et al, 1997;Baccus and Meister, 2002; Liu and Gollisch, 2015) we aimed to describe adaptation in contrast-responsive cells by fitting exponential models to the block-averaged activity in both contrasts. We were able to obtain significant fits (ANOVA, $p < 0.05$) in both contrast conditions for 295 (40%) of contrast-responsive cells. In another subset of 226 cells (31%), exponential adaptation was only present in one condition whereas in the other one, the activity trajectory was relatively flat. The remaining 205 (29%) responsive cells exhibited immediate jumps to a higher or lower activity state which was maintained for the duration of each block(Figure 2.A right) and thus could not be captured by an exponential model in either condition. We considered this last group of cells as one with fast contrast adaptation.

Within the subset of 295 cells with clear exponential-like adaptation in both contrasts, we found 2 major modes of slow adaptation. Similarly to retinal ganglion cells (Smirnakis et al, 1997;Baccus and Meister, 2002; Liu and Gollisch, 2015) and in agreement with studies on primary visual neurons that responded to oriented gratings (Sclar et al, 1990; Ghodrati et al, 2019), a number of neurons (n=62, 21%) increased their firing rate immediately after a step increment in contrast and decayed

to a lower steady state. For the same neurons, a step decrement in contrast induced an abrupt drop, followed by exponential recovery to a higher activity (Figure 2.A center graph). However, contrary to the aforementioned studies, we also found a strikingly larger number of cells (n=232, 78.6 %) that exhibited the reverse pattern of adaptation, i.e. increased firing rate, decaying to steady state after a transition to low contrast versus a transient initial suppression followed by recovery in high contrast (Figure 2.A left graph). Also, one exceptional cell was found to display decay to steady state following a transition to either condition. Interestingly, the relative prevalence of these modes of adaptation for each contrast had a clear association with cortical depth ($\chi^2(2) = 70.8065, p = 4.4409e-16$). We tested this hypothesis on the aggregate sample of 295 exponentially adapting cells with the subset of 226 that had exponential-like behaviour only in one contrast. The cells with decay in low contrast and/or recovery in high contrast dominated the supragranular layers (Figure 2.B), when examined in post-hoc comparisons with granular ($\chi^2(1) = 43.5971, p = 1.2103e-10$) and infragranular layers ($\chi^2(1) = 63.7888, p = 3.9969e-15$, with Bonferonni correction for multiple comparisons).

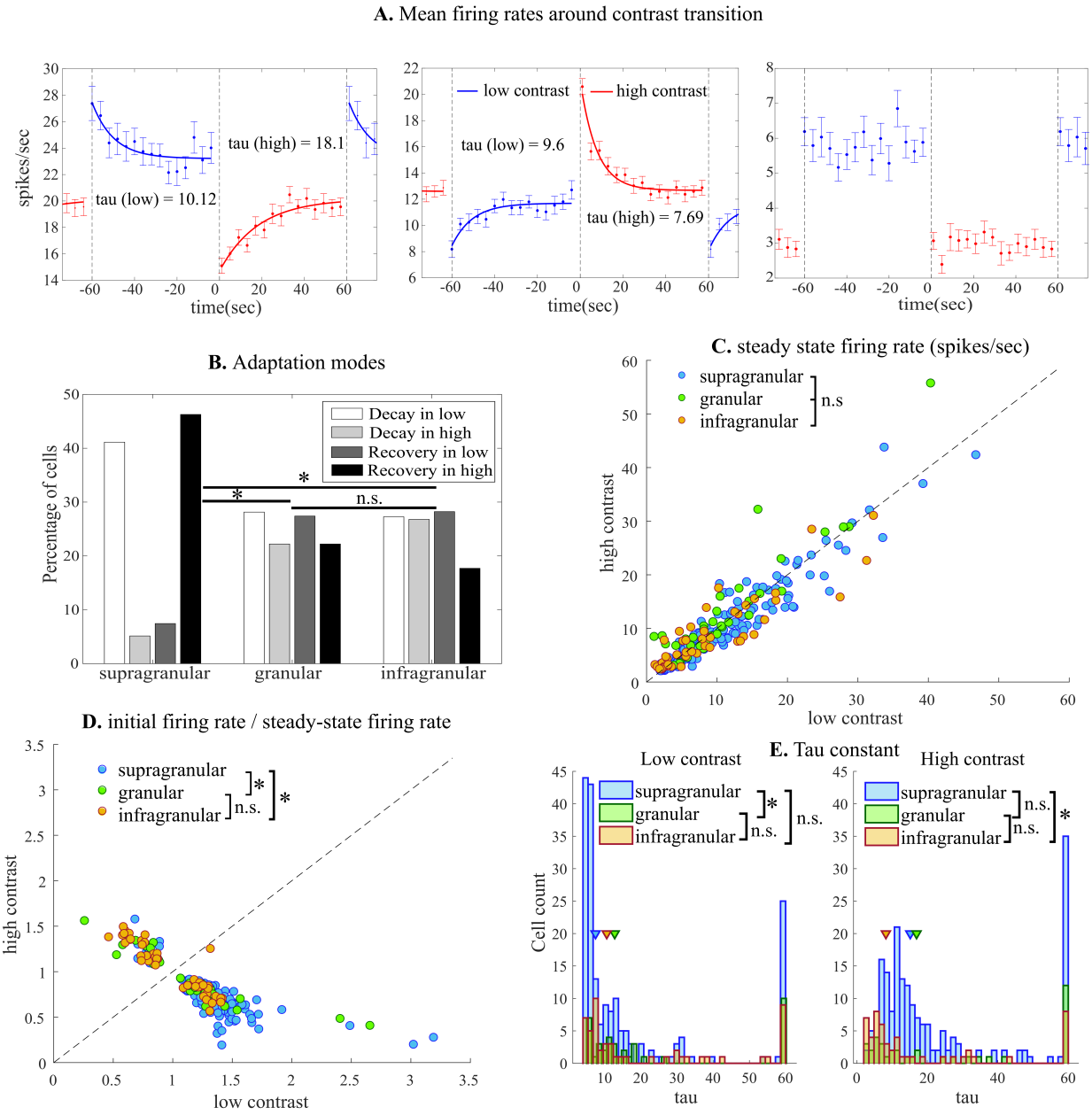

Figure 2: **The laminar profile of firing rate adaptation to contrast in primary visual cortex neurons A.** of slow and fast mean firing rate adaptation dynamics after a transition to low (blue) and to high contrast (red). Time is represented in seconds before and after a transition (t=0) from low to high contrast. Black vertical dashed lines indicate the borders between 60 sec blocks. Blue and red curves are the fitted exponential models to the firing rate profile after a transition to low versus high contrast. Tau: adaptation time constant τ. Error bars denote standard error of the mean. Segments beyond the [-60, 60] interval are periodic repetitions of the data. **B.** Distribution of cells with different firing rate adaptation modes across the cortical layers. To be included cells had to have at least one significant fit for one contrast transition. Percentages were calculated per layer. **C.** Scatter plot of steady state (60 seconds after a transition) firing rate at low (abscissa) vs high (ordinate) contrast. Distinct laminar domains are represented with different colors. **D.** Scatter plot of the ratio of the initial firing rate divided by the steady-state firing rate following a transition to low (abscissa) versus high (ordinate) contrast. Cells cluster in two different groups depending on the pattern of adaptation they exhibit. Distinct laminar domains are represented with different colors. **E.** Laminar distribution of the adaptation constant (τ), separately for each contrast condition.

Despite the contrast-induced changes that we observed in firing rates of individual exponentially-adapting cells (n=295), the adapted, steady state population-level activity did not differ significantly between contrasts for any laminar domain (Wilcoxon ranksum test, $p = 0.4145$ for supragranular, $p = 0.3889$ for granular and $p = 0.7341$ for infragranular cells). Pairwise 2-dimensional Kolmogorov-Smirnov tests with Bonferonni-adjusted p values for multiple comparisons further showed that this behaviour was uniform across layers ($KS = 0.2902, p = 0.369$, for supragranular vs granular layers,$KS = 0.1502, p = 0.99$, for supragranular vs infragranular layers and $KS = 0.2408, p = 0.99$, for granular vs infragranular layers). What contrast affected in this group of cells was the initial firing rate after a transition. We expressed the initial firing rate as a fraction of the steady-state rate at a given contrast level for each cell. This resulted in the formation of two clusters (Figure 2.D), which corresponded to the two major modes of slow adaptation (Figure 2.A left and middle). Not surprisingly, while granular and infragranular cells were scattered evenly across the two clusters (Wilcoxon ranksum test, $p = 0.9841$ for granular and $p = 0.4597$ for infragranular cells) supragranular cells mostly favoured higher initial activity in low contrast in conjuction with lower initial activity in high contrast ($p = 3.51e - 11$). These laminar differences were further confirmed by pairwise 2-dimensional Kolmogorov-Smirnov tests ($KS = 0.341, p = 0.0009$ for supragranular vs granular layers,$KS = 0.3164, p = 0.001$ for supragranular vs infragranular layers and $KS = 0.2239, p = 0.99$ for granular vs infragranular layers). Finally, the rate of adaptation as assessed by the τ constant varied wildly within the entire dataset. While all laminar populations had cells whose adaptation was either complete in the first few seconds or lasted and even exceeded the duration of the blocks, the rate of adaptation was differentially affected by contrast depending on laminar position. Specifically, the supragranular cells adapted faster than granular cells (Kruskal-Wallis test, $\chi^2 = 10.7462, p = 0.0046$, Bonferonni-adjusted post-hoc comparisons, $p = 0.0061$) but no other significant differences were observed. In high contrast, we found larger time constants in supragranular cells compared to infragranular cells(Kruskal-Wallis test, $\chi^2 = 10.0243, p = 0.0067$, Bonferonni-adjusted post-hoc comparisons, $p = 0.0045$), but all other differences were not significant. Cross-contrast tests for each layer separately, also revealed that supragranular cells exhibited faster adaptation in low contrast than in high contrast(Wilcoxon ranksum test, $p = 3.2961e - 12$), while granular and infragranular cells seemed to be unaffected by contrast (Wilcoxon ranksum test, $p = 0.8288$, for granular and $p = 0.1104$, for infragranular cells). However, since these contrast-induced changes could essentially reflect differences between the processes leading to decay and recovery, we also grouped and

compared cells in each layer according to the that distinction, regardless of contrast. We found that recovery was significantly slower than decay in supragranular (Wilcoxon ranksum test, $p = 1.0829e-11$) as well in infragranular (Wilcoxon ranksum test, $p = 8.1586e-05$), but not in granular cells (Wilcoxon ranksum test, $p = 0.7873$).

3.2 Contrast-dependent changes and laminar distribution of the STA parameters

We investigated the temporal feature tuning to full field contrast stimuli in macaque V1, by calculating the STA for all cells separately in low and high contrast. We were able to obtain significant STAs in both contrast conditions for 676 cells, as per the criterion described in the "Materials and Methods" section. Out of these cells, 526 could be assigned to a specific laminar domain and 507 (96%) of them were contrast-responsive. This final subset consisted of 281 supragranular, 124 granular and 121 infragranular cells. The shapes of the STAs varied from monophasic to multiphasic (Figure 3.A) although the majority of them were biphasic or triphasic (Figure 3.B). We found no significant association between the proportions of STA types and laminar position either in low ($\chi^2(6) = 0.062, p = 0.99,$) or high contrast ($\chi^2(6) = 0.0454, p = 0.99,$). Furthermore, these proportions were similarly unaffected by contrast level within supragranular ($\chi^2(3) = 0.0399, p = 0.99,$), granular ($\chi^2(3) = 0.037, p = 0.99,$) and infragranular populations ($\chi^2 = 0.1383, p = 0.98,$).

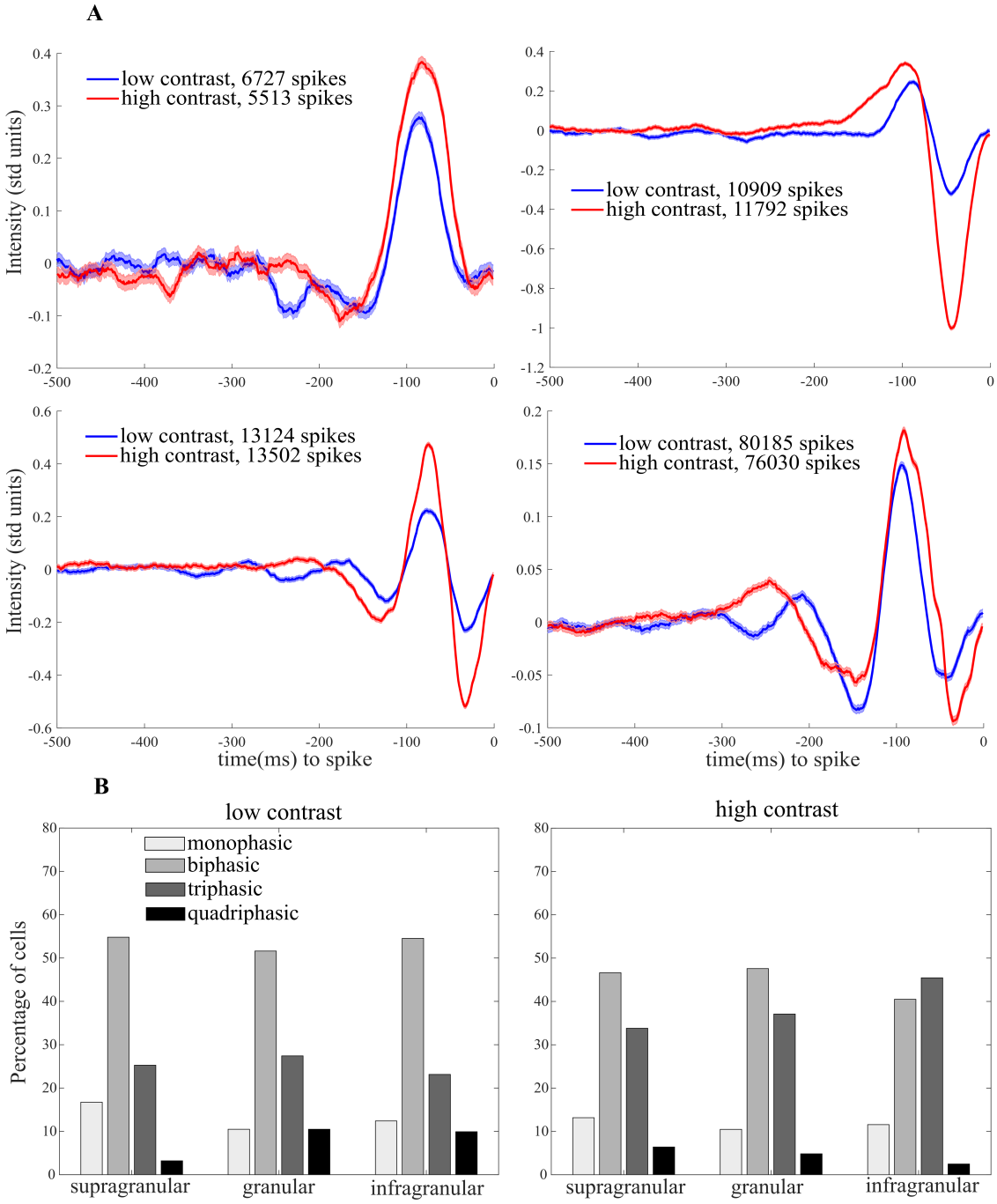

Figure 3: **Temporal filters adapt to changes in contrast A.** Four spike-triggered average examples in low (blue) and high (red) contrast. Spike triggered values are expressed as deviations from the mean intensity normalized to unit standard deviation, and are computed separately for low and high contrast. Shaded regions around the curves represent the standard error of the mean. The number of spikes used for computing each STA is shown in the legend. A time interval of 500 milliseconds before the spike occurrence at t=0, is plotted here. Typical STAs exhibit positive and/or negative peaks within a 500ms temporal window preceding the spike and gradually approximate the mean at longer time delays. The number of peaks observed varied from one (monophasic, top left graph) to four (quadriphasic, bottom right graph). **B.** Bar graph of the proportion of different STA types across cortical depths .

Despite this trend, when we examined how individual cells behaved between contrast levels, we found that only approximately half of the entire sample retained the same number of peaks (Figure 4.C). The other half either gained or lost a positive or negative peak from low to high contrast, which suggested qualitative changes in temporal filtering as a function of contrast, that are not only differences in filter scale. Two such examples of cells with markedly different behaviour between contrasts are provided in Figure 4.B.

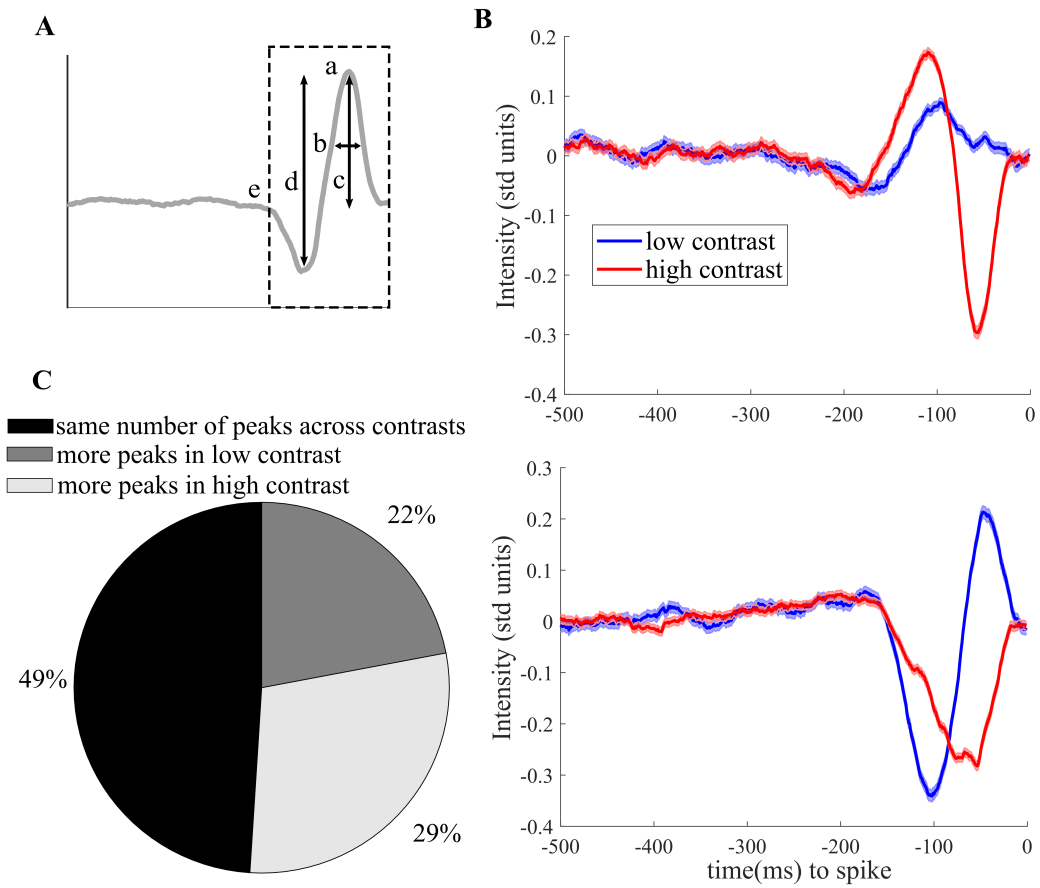

Figure 4: **Temporal STA profiles are not always the same across contrasts. A.** Parameter extraction for the STA: a: Time to peak, b: width of peak at half-amplitude, c: amplitude of peak, d: peak-to-peak amplitude, e: integration window of the STA, illustrated as the part of the filter that is enclosed in the dashed rectangle. **B.** Examples of cells with STAs that gained (top graph) or lost peaks (bottom graph) from low to high contrast. **C.** Pie chart illustrating the percentages of cells that retain or change their temporal processing profiles in terms of number of peaks across contrasts.

In order to characterize contrast-dependent STA parameter alterations and perform comparisons across cortical layers, we restricted our analysis to biphasic cells that displayed peaks of corresponding positive or negative polarity between contrasts. A subset of 180 cells satisfied this criterion, out of which, 76 were supragranular, 30 were granular, 34 were infragranular and the rest 40 were in border

regions between layers and thus were excluded from the analysis. We further divided these cells into those that had a positive first peak (n=69) and those that had a negative first peak (n=71). Then, we tested for the effect of contrast on every time-domain STA peak parameter in each layer. Moreover, we performed pairwise Kolmogorov-Smirnov tests with Bonferroni-adjusted p values on the laminar cross-contrast distributions of the STA parameters (Figure 5).

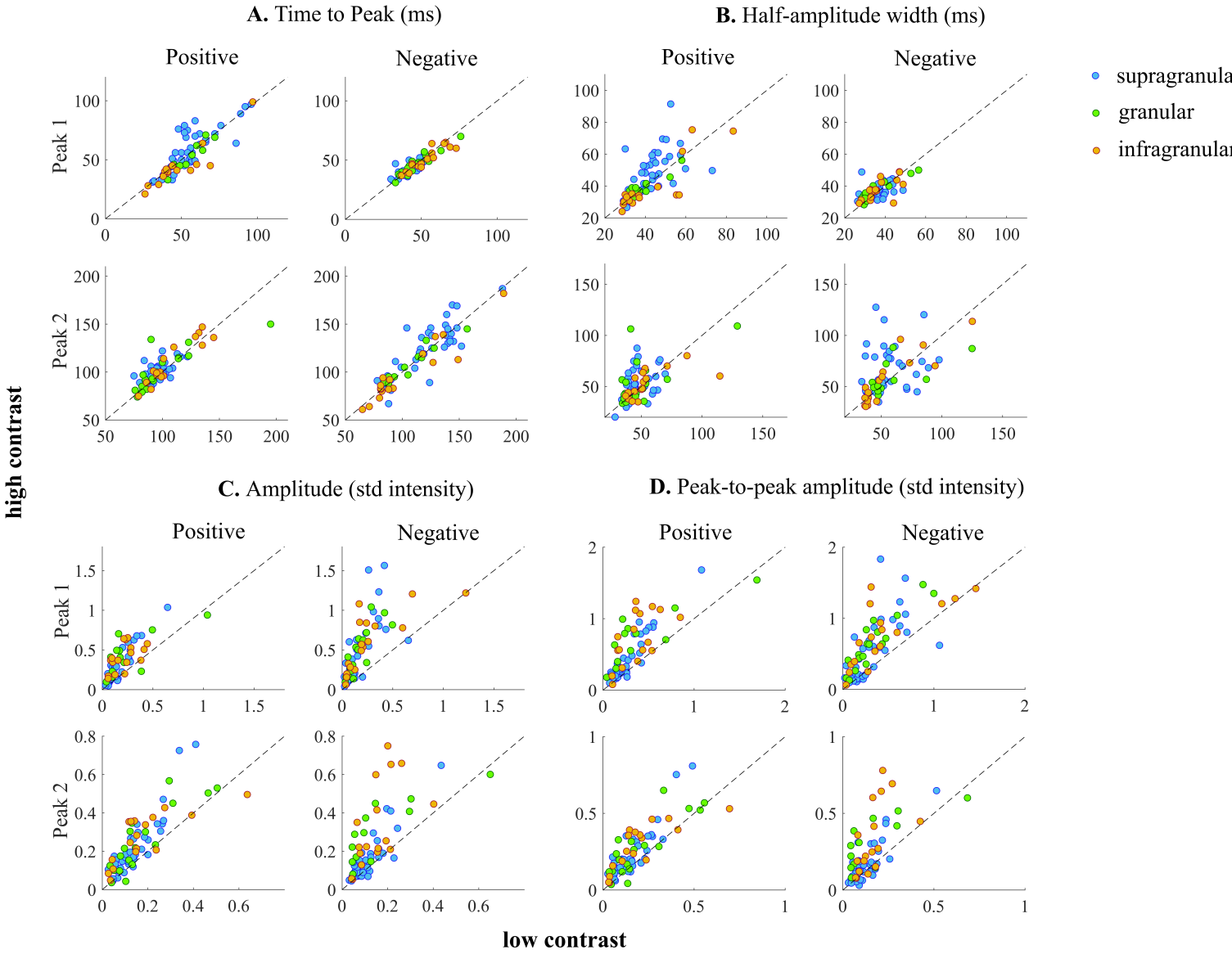

Figure 5: **Distributions of STA peak parameters across the cortical layers. A.** Time to Peak in ms. **B.** Width at half amplitude in ms. **C.** Peak amplitude in std units of the stimulus intensity. **D.** Peak-to-peak amplitude in std units of the stimulus intensity. All x axes represent parameter values measured in low contrast and all y axes represent such values in high contrast. Black dashed lines denote the identity line. Every comparison for the first and the second peak was made separately depending on the peak polarity. Colour conventions for the laminar domains are the same as in Figure 2.

Despite the fact that we scaled the STAs with the standard deviation of each contrast condition, we still found that raising the contrast induced a significant increase in the amplitude (Figure 5.C) and peak-to-peak amplitude (Figure 5.D) of the peaks. This signified a decrease in temporal feature sensitivity at high contrasts, that exceeded what would be expected if the filter was scaled proportionately with the change in contrast. This change was observed in all cortical layers and for all peaks regardless of polarity and proximity to spike (24 Wilcoxon rank sum tests for all layers and peak categories for which $p < 0.05$). Moreover, this effect was uniform across the cortical layers as shown by subsequent sets of pairwise Kolmogorov-Smirnov tests in each peak category ($p > 0.05$). Contrary to the above, the time to peak (Figure 5.A) and the half-amplitude width (Figure 5.B) were not altered significantly by contrast in any peak category or laminar domain (24 Wilcoxon rank sum tests for all layers and peak categories for which $p > 0.05$). However, we found significant paiwise differences between the 2-dimensional cross-contrast distributions of the supragranular and the infragranular cells only in the case of the first positive peak ($KS = 0.5985, p = 0.019$, for the time to peak and $KS = 0.6147, p = 0.013$, for the peak width) .

3.3 Contrast-dependent changes in the response function

We computed the effective stimulus for each cell by projecting the stimulus onto the STAs separately in each contrast condition. The resulting values for both contrasts were normalized with the standard deviation of the effective stimulus distribution at low contrast. Then, we fitted the responses as a function of the effective stimulus with sigmoid models. We were able to obtain significant fits for 453 cells (ANOVA test, $p < 0.05$), out of which 244 were located in supragranular, 105 in granular and 104 in infragranular layers. The responses were predominantly simple-cell-like sigmoid curves that displayed baseline activity at negative effective stimulus values (i.e. temporal modulations of the stimulus that are roughly in opposite direction to the modulation seen in the STA) and peaked towards larger correlations with the STA (positive semi-axis). Most cells ($N = 310, 69\%$) retained their sigmoid response profiles in both contrasts, albeit with rescaling the parameters (Figure 6.A, top left). A minority of cells displayed more complex-cell-like responses in both contrasts, i.e. sigmoid modulation for positive and negative effective stimulus values alike, in the form of symmetric excitation ($N = 10, 2.2\%$) as in the example of Figure 6.A bottom right or symmetric suppression ($N = 9, 2\%$)shown in Figure 6.A

bottom left. Finally, a number of other cells displayed more remarkable changes with contrast as their sigmoid response in low contrast was transformed to a symmetric one of either excitation (Figure 6.A, top right) ($N = 90, 20\%$) or suppression ($N = 34, 7.5\%$) in high contrast. As with the types of STA, the distributions of response types were similar across the layers (Figure 6.C) both in low ($\chi^2(2) = 2.0562, p = 0.725,$) and high contrast ($\chi^2(2) = 8.0565, p = 0.089$). However, when we examined the effect of contrast on these response types, we found significant changes in their relative proportions in supragranular ($\chi^2 = 22.1823, p = 1.5246e{-}5$), granular ($\chi^2 = 34.0922, p = 3.9535e{-}8$) and infragranular layers ($\chi^2 = 14.3929, p = 7.4924e-4,$). High contrast seemed to introduce a greater degree of nonlinear behaviour even among cells that had regular sigmoid responses in low contrast(Figure 6.C).

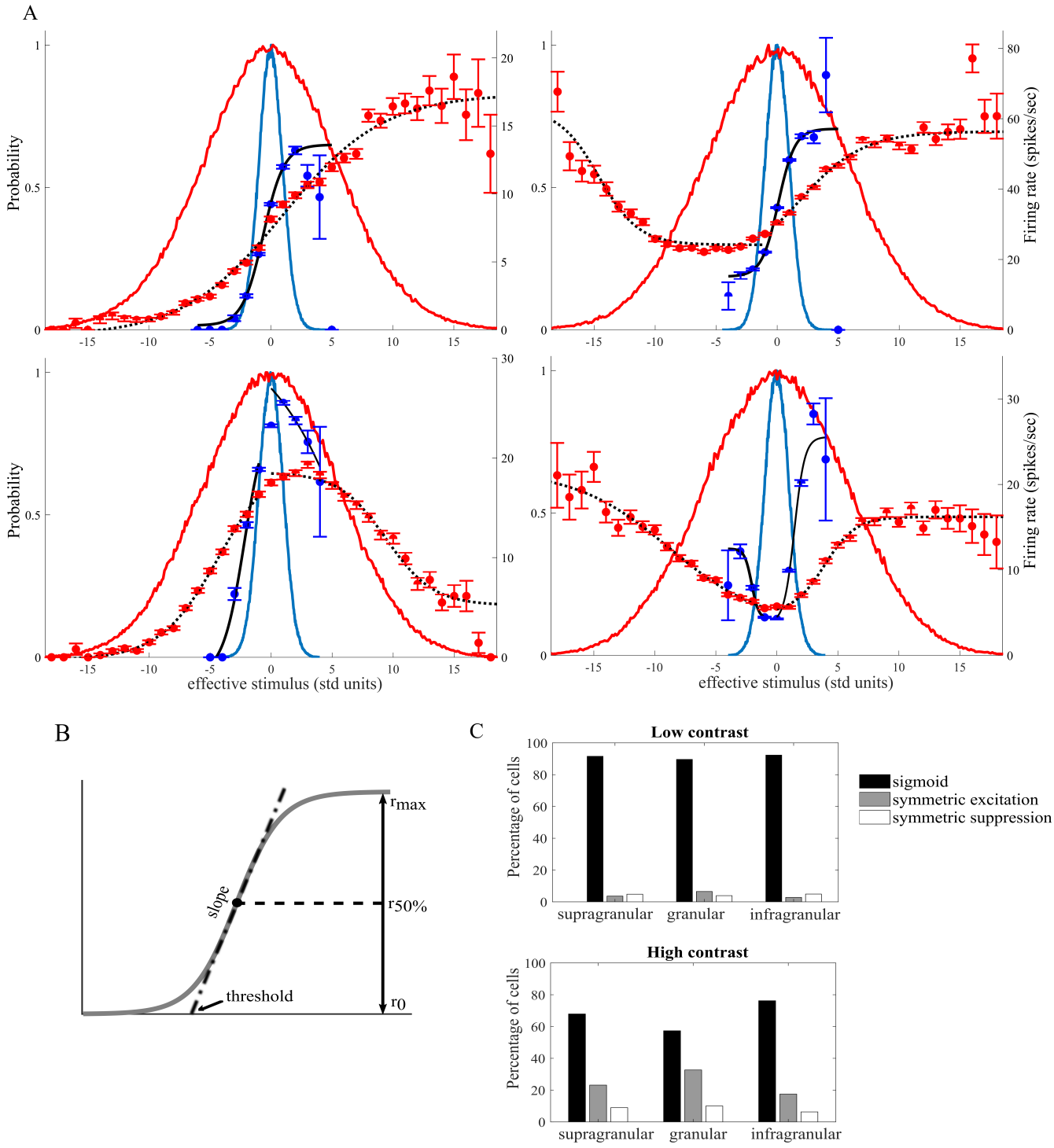

Figure 6: **Effective Stimulus Response Functions A.** Four cells with different effective stimulus response functions, in low (blue) vs high (red) contrast conditions. Effective stimulus values (x axis) are in units of standard deviation of the low contrast distribution. Left y axis: frequency of effective stimulus values, normalized so that the peak of the distribution is one. Right y axis: firing rate in spikes/sec (Hz). Colored dots denote the cells response to the corresponding effective stimulus values (blue: low, red: high contrast). Error bars indicate standard error of the mean. Solid black curve: fit for low contrast responses. Dotted black curve: fit for high contrast responses. **B.** Parameters of the effective stimulus response function. **C.** Distribution of effective stimulus response types across the cortical depths for low and high contrast.

As previous reports documented (Ozhawa et al, 1982; Ozhawa et al, 1985; Sclar et al,1989), adaptation to luminance contrast involves changes in the cell's sensitivity to deviations in light intensity. These changes might affect the operating range where a cell exhibits graded responses by adjusting the slope at the half-maximum of the sigmoid curve or the effective threshold which signifies the point in the effective stimulus where these graded responses take off. To capture the extent of the changes in the operating range, we expressed both the low and high contrast effective stimulus distributions in units of standard deviation of the low contrast one. Contrast-induced changes might also alter the predicted dynamic range or shift the baseline of a cell by adjusting the maximum and minimum predicted firing rate of the sigmoid curve. Our analysis showed that primary visual neurons in the macaque display all the aforementioned effects to an extent. We conducted this stage of the analysis separately for two cells groups, a first one of the 310 cells with simple-cell response functions (Figure 7.A-D main plots) and a second one with the aggregate set of 143 cells with complex-cell responses either in one or both contrasts (Figure 7.A-D insets). For the second group, the comparisons were based on parameters extracted from sigmoid curves with baseline modulation at smaller effective stimulus values and maximum modulation at larger ones.

Firstly, the slope at the half-maximum was strikingly smaller in high contrast relative to low contrast. This was uniformly expressed in both cell groups (Figure 7.A, main plot and inset) and in all cortical layers as supragranular, granular and infragranular cells significantly reduced their slopes by a median factor of 3.6, 3.5 and 3.3 respectively for the first cell group (Wilcoxon rank sum test, $p = 5.163e-28, p = 1.019e-16$ and $p = 2.989e-20$) and 2.7, 3.2 and 4.6 respectively for the second group (Wilcoxon rank sum test, $p = 4.729e-17, p = 8.465e-10$ and $p = 1.415e-05$). Subsequent pairwise Kolmogorov-Smirnov tests confirmed the uniform character of this change for all layers in V1 in both cell groups ($KS = 0.1876, p = 0.3170$, $KS = 0.3028, p = 0.0777$, for supragranular versus granular cells in first and second group respectively, $KS = 0.2028, p = 0.1233$, $KS = 0.3810, p = 0.0812$ for supragranular versus infragranular cells in first and second group respectively and $KS = 0.1495, p = 0.99$, $KS = 0.2424, p = 0.99$ for granular versus infragranular cells in first and second group respectively). Upward changes in stimulus contrast also induced adaptive changes in the effective threshold of supragranular cells in both groups. The thresholds at high contrast in these populations were shifted towards the negative semi-axis by a median of 4.5 (first cell group, Figure 7.B main plot) (Wilcoxon rank sum test, $p = 3.2381e-11$) and 2.6 (second cell group, Figure 7.B inset) (Wilcoxon rank sum test, $p = 2.9967e-7$)

standard deviation units of effective stimulus. However, granular and infragranular thresholds in both cell groups remained relatively unchanged by contrast (Wilcoxon rank sum test, $p = 0.6354$, $p = 0.0545$ for granular cells of the first and second group respectively and $p = 0.3054$, $p = 0.0585e$ for infragranular cells of the first and second group respectively).

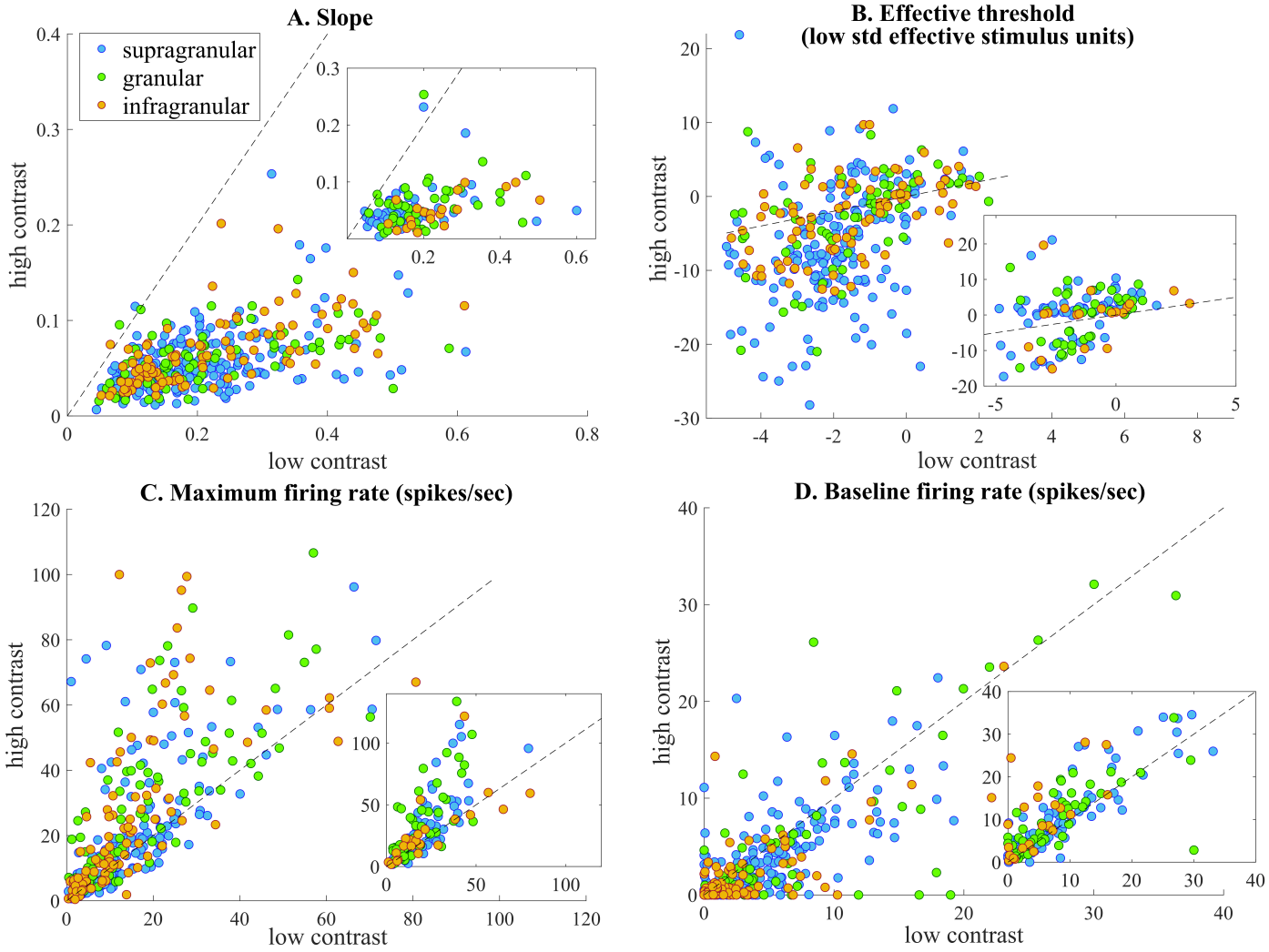

Figure 7: Distribution of effective stimulus response parameters for low and high contrast across the cortical layers. All main scatter plots illustrate the distributions for cells with sigmoid response functions whereas inset plots represent the same distributions for all other cells. **A.** The slope at half maximum of the sigmoid fit, with the maximal firing rate plateau normalized to 1. **B.** The effective threshold, i.e. the x-axis intercept of the linear part of the sigmoidal fit, where responses to effective stimulus begin to rise. **C, D.** Maximum and minimum (baseline) firing rates from the upper and lower plateaus of the sigmoid model. Axes and color conventions are the same as in figure 5.

Contrast-dependent changes were observed in the response range of the sigmoid curves. Interestingly, granular cells in the first and second group raised their maximum modulation plateau in high contrast on a median level from 16.9 to 30.7 (Figure 7.C, main plot) (Wilcoxon ranksum test, $p = 0.0081$) and

from 14.4 to 18.5 spikes per second (Figure 7.C, inset) (Wilcoxon ranksum test, $p = 0.0274$) respectively. Infragranular cells also followed that trend but only for the first cell group, as they raised their maximum plateau on a median level from 10.4 to 16.5 spikes per second (Wilcoxon ranksum test, $p = 0.0274$). No other significant differences were observed regarding this parameter. Lastly, contrast induced some small but statistically significant shifts in the predicted baseline responses for the supragranular and infragranular cells of the first group but left the rest of the cell populations unaffected. While a degree of variability was present in these changes low contrast baseline rate was overall higher than in high contrast by a median of 1.5 spikes per second for both supragranular (Wilcoxon ranksum test, $p = 0.0069$) and infragranular cells (Wilcoxon ranksum test, $p = 0.0109$).

3.4 Adaptation dynamics of the linear-nonlinear models

Since contrast adaptation has been shown to involve both fast and slow components (Ozhawa et al, 1982; Ozhawa et al ,1985; Ghodrati et al, 2019), we investigated the temporal dynamics of the parameters of the STA and the nonlinearity during adaptation by carrying out the same analysis, as in steady-state, but in 10 successive 6-second bins for every contrast condition. Most neurons in this analysis, exhibited variable quality regarding the STAs and response functions throughout the entire 60 second interval. Therefore, we chose to track differences between only the early phase of adaptation (0-6 seconds) and the steady-state. The steady-state in this analysis was defined as the last 24 seconds in a contrast block, so as to have more reliable estimates. As a first stage, we were able to confirm previous results on the fast time-scale of STA adaptation (Sharpee et al, 2006; Ghodrati et al, 2019). As in previous reports, no significant differences were found between any of the parameters that were extracted during the early adaptive stage (0-6 secs) and the steady state, in any laminar cell population (Wilcoxon ranksum test, $p > 0.05$). This indicated that contrast-dependent changes in the STA waveform, happened on a faster time-scale than our temporal resolution could capture. As for the response function, we found 169 cells that could be significantly fitted (ANOVA, $p < 0.05$) with a single or a combination of sigmoid models, at both phases of the adaptation. Since the dynamics of the response function could be related to the dynamics of firing rate adaptation, we separated the cells into a group that displayed exponential decay after a contrast transition (Figure 8.A low contrast and Figure 8.B high contrast), another one that displayed exponential recovery (Figure 8.A high contrast and Figure 8.B low contrast) and a third one

that consisted of cells which showed fast or no adaptation to contrast, and were therefore not expected to change between the early adaptive stage and the steady state.

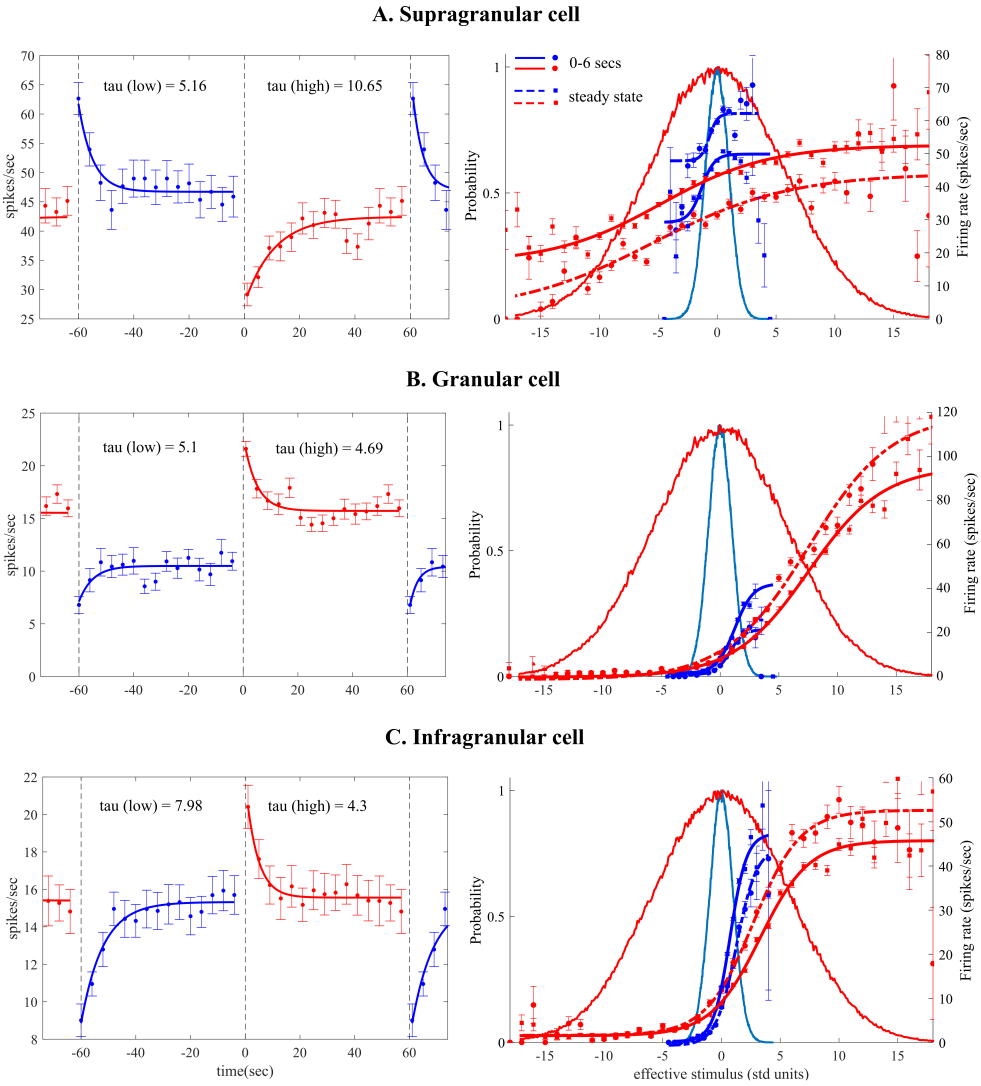

Figure 8: **Examples of adaptation to contrast. A.** Example of a supragranular cell's mean firing rate around contrast transitions and response function from the first 6 seconds and the steady state. For this cell, the maximum and minimum firing plateau appear to be the chief sigmoid parameters that change from 0-6sec post contrast transition to steady state.**B.** Same plots for a granular cell that changes only its maximum firing plateau from the first six seconds to the steady-state phase of adaptation **C.** Same plots for an infragranular cell whose effective response function shows little change following a low contrast transition, compared to a change in slope and a shift in the maximum firing plateau following a transition to high contrast. All conventions are the same as in figures 2, 3 and 6

Some individual cells showed slow adaptive changes within a contrast block that took the form of either a translational baseline shift (Figure 8.A) or a change in the dynamic response range (Figure 8.B). However, there were large variations to this behaviour which resulted in a mixed picture at the

level of the population (Figure 9). In order to test the trends in the population we conducted mixed factorial ANOVA test by considering the phase of the adaptation as a within-subject factor and the mode (i.e. decay, recovery and fast or no adaptation) and cortical depth as between-subject factors. We found no significant main effects on any of the aforementioned factors ($p > 0.05$). Notably, the group of cells whose mean spiking activity adapted rapidly or did not change as a function of contrast, showed similar variation to the other two groups in virtually every parameter difference that we measured. This was probably an indication that the quality of the fitted sigmoid models deteriorated when the response functions were estimated in 6-second time bins. As a result, this level of noise could have rendered any potential subtle differences undetectable.

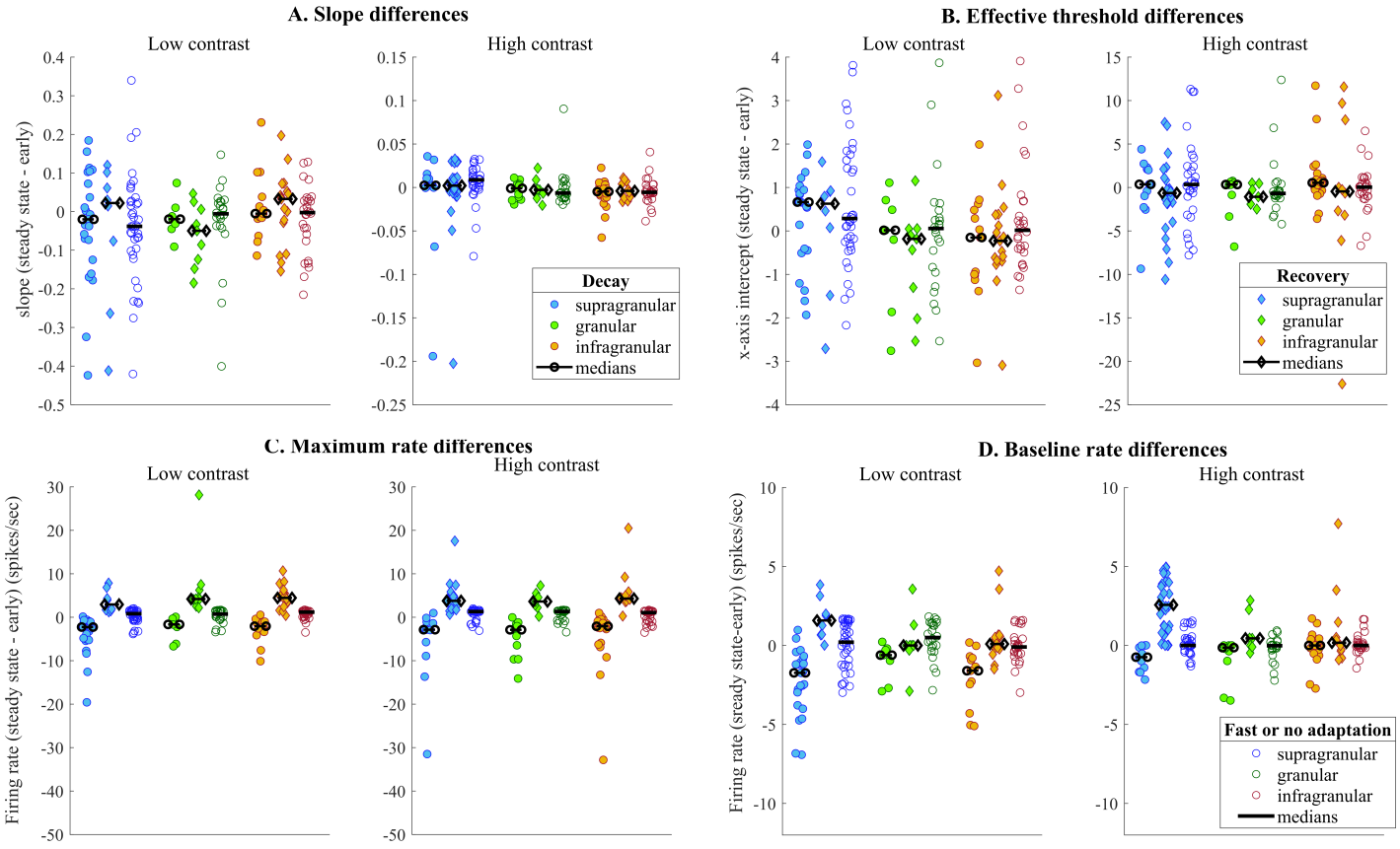

Figure 9: Adaptation of the parameters of the response function. Scatter plots depict pairwise differences of the response parameters from measurements during the early phase (0-6 secs) and the steady state (42-60 secs) for every cell across the cortical depths. The cells were separated into 3 categories depending on adaptation mode in eah contrast, namely decay (filled circles), recovery (filled diamonds) and fast or no adaptation (hollow circles). **A, B.** Differences in the slope and the effective threshold. **C, D.** Differences in the maximum and minimum (baseline) plateaus from the sigmoid fits. The dispersion along the x-axis for each of the laminar distributions does not represent any feature of the data, but is solely for a clearer illustration of the sample densities. Medians per cortical depth are denoted with black horizontal lines with circle, diamond or no marker for decay, recovery and fast or no adaptation respectively. All other conventions are the same as in Figures 2, 3 and 6.

4 Discussion

Contrast adaptation is a process of fundamental importance for the early visual system. In this study, we investigated how contrast shapes linear-nonlinear descriptions of single-cell encoding in V1 using a simplified uniform-field flicker stimulus in low and high contrast. We also asked whether the features of these encoding descriptions are in any respect different among different layers of the macaque primary visual cortex. Our findings revealed a previously undiscovered rich set of contrast-dependent changes

in the mean activity adaptation dynamics, temporal filtering (STA) and the responsivity to contrast (effective stimulus response function). Interestingly, raising the contrast did not only result in scaled versions of the STAs and the nonlinearities, but also induced, in some cases, qualitative changes that transformed temporal feature tuning and polarity dependence of response. Furthermore, while the majority of cells modulated their activity in response to upward and downward steps in contrast, the time-scale and the modes of adaptation varied considerably across the population. Despite that, most population-level parameter alterations in the STA and the response function happened within the first few seconds following a contrast transition. Finally, we found that contrast adaptation is to a certain extent, not a uniform phenomenon across all cortical depths, as the parameters of the mean firing rate dynamics and the response functions varied considerably depending on laminar location.

A widely held view is that cells in the visual pathway adapt to different contrast conditions such that their spatiotemporal encoding properties remain invariant with respect to contrast (Movshon et al, 1978; Albrecht and Hamilton, 1982; (Nowak and Barone, 2009); (Berens et al., 2012)). It has also been suggested that contrast invariance can be attained with divisive normalization of cell responses ((Carandini and Heeger, 2012)). However, various studies have presented evidence against contrast invariance for spatial summation, spatial frequency tuning and orientation selectivity ((Sceniak et al., 1999); (Sceniak et al., 2002); (Durand et al., 2012); (Lee et al., 2019)) as well as for temporal visual features such as temporal frequency tuning and high-frequency cut-offs ((Holub and Morton-Gibson, 1981); (Dean and Tolhurst, 1986); (Reid et al., 1992); (Hawken et al., 1996)). Our findings lend further support against invariance. The preferred temporal visual features in our data did not scale proportionately with the contrast level as would be predicted by frameworks that advocate gain control through normalization ((Heeger, 1992); Carandini and Heeger, 2012). Instead, peak amplitudes and peak-to-peak amplitudes were significantly larger in high than in low contrast for all laminar domains (Figure 5.C-D), despite the fact that STAs were scaled by the standard deviation of their respective stimulus ensembles. An even stronger case against invariance can be made with the qualitative contrast-induced changes in a considerable portion of our sample, that fundamentally altered the temporal filtering profile (Figure 4.B-C) and the response function (Figure 6.C).

Contrast adaptation manifests in various aspects of neural function and operates over multiple time-scales (reviewed in (Wark et al., 2007)). In correspondence with previous studies (Ozhawa et al, 1982; Ozhawa et al, 1985; Baccus and Meister, 2002; (Sharpee et al., 2006); Ghodrati et al, 2019) we found that

contrast induced rapid changes in the STAs. This was despite the fact that the firing rate could reach steady state comparably fast, within few seconds or several seconds after contrast transition (Figure 2.E). However, we found that most contrast-dependent changes in the effective stimulus response function had a homogeneously faster time course than the firing rate, or did not consistently follow the slow dynamics of the firing rate adaptation (Figure 9). It should be noted, though, that the inconsistency might have resulted from lower signal-to-noise ratio due to fewer spikes in the case of 6-second bins. One of our most remarkable findings was the staggering presence of cells that adapted to low contrast by decaying from a higher activity and to high contrast by recovering to a higher steady state after a transient initial drop. Although this is the reverse pattern of what was previously observed (Smirnakis et al, 1997; Baccus and Meister, 2002; Liu and Gollisch, 2015), recovery in high contrast has been reported in previous work (Albrecht and Hamilton, 1984) but was less prevalent in the population than what we show here. Moreover, the high-contrast steady state of these neurons in Albrecht and Hamilton (1984) was still higher than in low contrast, whereas the same sample in our study had mostly comparable or lower activity at steady state in high compared to low contrast. Furthermore, with the exception of granular cells, we found recovery to be significantly slower than decay regardless of contrast level, which could imply that they are driven by different processes.

A mechanistic understanding of contrast-dependent encoding in V1 is still missing in the literature. A first step towards that would be to identify how encoding descriptions might differ across the V1 cortical layers. We found such differences in the firing rate adaptation and the steady-state effective stimulus response functions but not for the STAs. Past work on temporal filtering was similarly unable to detect laminar differences in temporal frequency tuning but contrary to our investigation, they also found the granular population exhibited more lowpass filtering and shorter integration times than in other layers (Hawken et al, 1996). While laminar and cell-type differences in response functions were not found in previous studies (Ozhawa et al 1985; (Cavanaugh et al., 2002)), we uncovered differences that could potentially group our cell sample into functionally distinct categories. Supragranular cells could form the first category as they adapt to contrast changes by changing their contrast operating range through significant adjustments both in the response slope and the effective threshold (Figure 7.A-B). The second category could consist of granular and infragranular cells together as their contrast adaptation combines changes both in the operating range as well as the response range (Figure 7.A, 7.C). The laminar distribution of the two major modes of firing rate adaptation which were equally

present in granular and infragranular but strikingly imbalanced in supragranular layers (Figure 2.B) provides additional support to this division.

What could be the mechanism that endows different properties to cells from different layers in V1? Anatomical studies (reviewed in Callaway, 1998) have shown that granular and infragranular layers to a smaller extent, receive direct magnocellular inputs from the lateral geniculate nucleus whereas supragranular do not. But there is also a functional account for the properties that we observed, and that is related to surround modulation. Given that the stimulation was uniform and full-field, cell responses were a product of interaction between the classical receptive field and the extraclassical one or the surround. These two have been proposed to operate with separate mechanisms where the relative influence of each is determined by a gain parameter (Cavanaugh and Bair, 2002). When the surround gain is higher, the cell's response is suppressed. Surround stimulation has been demonstrated to evoke greater suppression when the stimulus in the receptive field is of high contrast and to be potentially facilitatory in low contrast (Sceniak et al, 1999; Cavanaugh and Bair, 2002). Furthermore, surround suppression is stronger in supragranular layers compared to infragranular and granular layers (reviewed in (Angelucci et al., 2017)). Considering all the aforementioned, it is reasonable to suggest that cells which decreased their firing rate in high contrast and were massively present in the supragranular layers, did so due to surround modulation effects.

5 References

References

Albrecht, D., Farrar, S., and Hamilton, D. (1984). Spatial contrast adaptation characteristics of neurones recorded in the cat's visual cortex. *J Physiol*, 347(1):713–739.

Albrecht, D. G. (1995). Visual cortex neurons in monkey and cat: effect of contrast on the spatial and temporal phase transfer functions. *Vis Neurosci*, 12(6):1191–1210.

Albrecht, D. G. and Geisler, W. S. (1991). Motion selectivity and the contrast-response function of simple cells in the visual cortex. *Vis Neurosci*, 7(6):531–546.

547 Anderson, J. S., Lampl, I., Gillespie, D. C., and Ferster, D. (2000). The contribution of noise to contrast
548 invariance of orientation tuning in cat visual cortex. *Science*, 290(5498):1968–1972.

549 Angelucci, A., Bijanzadeh, M., Nurminen, L., Federer, F., Merlin, S., and Bressloff, P. C. (2017). Circuits
550 and mechanisms for surround modulation in visual cortex. *Annu Rev Neurosci*, 40:425–451.

551 Baccus, S. A. and Meister, M. (2002). Fast and slow contrast adaptation in retinal circuitry. *Neuron*,
552 36(5):909–919.

553 Barlow, H. B. et al. (1961). Possible principles underlying the transformation of sensory messages.
554 *Sensory communication*, 1:217–234.

555 Berens, P., Ecker, A. S., Cotton, R. J., Ma, W. J., Bethge, M., and Tolias, A. S. (2012). A fast and
556 simple population code for orientation in primate v1. *J Neurosci*, 32(31):10618–10626.

557 Callaway, E. M. (1998). Local circuits in primary visual cortex of the macaque monkey. *Annu Rev*
558 *Neurosci*, 21(1):47–74.

559 Carandini, M. and Heeger, D. J. (2012). Normalization as a canonical neural computation. *Nat Rev*
560 *Neurosci*, 13(1):51.

561 Carandini, M., Heeger, D. J., and Senn, W. (2002). A synaptic explanation of suppression in visual
562 cortex. *J Neurosci*, 22(22):10053–10065.

563 Cavanaugh, J. R., Bair, W., and Movshon, J. A. (2002). Nature and interaction of signals from the
564 receptive field center and surround in macaque v1 neurons. *J Neurophysiol*, 88(5):2530–2546.

565 Chance, F. S., Nelson, S. B., and Abbott, L. F. (1998). Synaptic depression and the temporal response
566 characteristics of v1 cells. *J Neurosci*, 18(12):4785–4799.

567 Chander, D. and Chichilnisky, E. (2001). Adaptation to temporal contrast in primate and salamander
568 retina. *J Neurosci*, 21(24):9904–9916.

569 Chao-Yi, L. and Creutzfeldt, O. (1984). The representation of contrast and other stimulus parameters
570 by single neurons in area 17 of the cat. *Pflügers Archiv*, 401(3):304–314.

571 Dean, A. and Tolhurst, D. (1986). Factors influencing the temporal phase of response to bar and grating
572 stimuli for simple cells in the cat striate cortex. *Exp Brain Res*, 62(1):143–151.

573 Durand, J.-B., Girard, P., Barone, P., Bullier, J., and Nowak, L. G. (2012). Effects of contrast and
574 contrast adaptation on static receptive field features in macaque area v1. *J Neurophysiol*, 108(7):2033–
575 2050.

576 Ghodrati, M., Zavitz, E., Rosa, M. G., and Price, N. S. (2019). Contrast and luminance adaptation
577 alter neuronal coding and perception of stimulus orientation. *Nat Commun*, 10(1):941.

578 Hawken, M., Shapley, R. M., and Grosof, D. (1996). Temporal-frequency selectivity in monkey visual
579 cortex. *Vis Neurosci*, 13(3):477–492.

580 Heeger, D. J. (1992). Normalization of cell responses in cat striate cortex. *Vis Neurosci*, 9(2):181–197.

581 Holub, R. and Morton-Gibson, M. (1981). Response of visual cortical neurons of the cat to moving
582 sinusoidal gratings: response-contrast functions and spatiotemporal interactions. *J Neurophysiol*,
583 46(6):1244–1259.

584 Laughlin, S. (1981). A simple coding procedure enhances a neuron's information capacity. *Z Naturforsch*
585 *[C]*, 36(9-10):910–912.

586 Lee, S., Park, J., and Smirnakis, S. M. (2019). Internal gain modulations, but not changes in stimulus
587 contrast, preserve the neural code. *J Neurosci*, 39(9):1671–1687.

588 Nowak, L. G. and Barone, P. (2009). Contrast adaptation contributes to contrast-invariance of orienta-
589 tion tuning of primate v1 cells. *PLoS One*, 4(3):e4781.

590 Ohzawa, I., Sclar, G., and Freeman, R. (1982). Contrast gain control in the cat visual cortex. *Nature*,
591 298(5871):266.

592 Ohzawa, I., Sclar, G., and Freeman, R. D. (1985). Contrast gain control in the cat's visual system. *J*
593 *Neurophysiol*, 54(3):651–667.

594 Reid, R., Victor, J., and Shapley, R. (1992). Broadband temporal stimuli decrease the integration time
595 of neurons in cat striate cortex. *Vis Neurosci*, 9(1):39–45.

Sceniak, M. P., Hawken, M. J., and Shapley, R. (2002). Contrast-dependent changes in spatial frequency tuning of macaque v1 neurons: effects of a changing receptive field size. *J Neurophysiol*, 88(3):1363–1373.

Sceniak, M. P., Ringach, D. L., Hawken, M. J., and Shapley, R. (1999). Contrast's effect on spatial summation by macaque v1 neurons. *Nat Neurosci*, 2(8):733.

Schmolesky, M. T., Wang, Y., Hanes, D. P., Thompson, K. G., Leutgeb, S., Schall, J. D., and Leventhal, A. G. (1998). Signal timing across the macaque visual system. *J Neurophysiol*, 79(6):3272–3278.

Schwartz, O., Pillow, J. W., Rust, N. C., and Simoncelli, E. P. (2006). Spike-triggered neural characterization. *J Vis*, 6(4):13–13.

Sclar, G. and Freeman, R. (1982). Orientation selectivity in the cat's striate cortex is invariant with stimulus contrast. *Exp Brain Res*, 46(3):457–461.

Sclar, G., Lennie, P., and DePriest, D. D. (1989). Contrast adaptation in striate cortex of macaque. *Vision Res*, 29(7):747–755.

Self, M. W., van Kerkoerle, T., Supèr, H., and Roelfsema, P. R. (2013). Distinct roles of the cortical layers of area v1 in figure-ground segregation. *Curr Biol*, 23(21):2121–2129.

Shapley, R. M. and Victor, J. D. (1978). The effect of contrast on the transfer properties of cat retinal ganglion cells. *J Physiol*, 285(1):275–298.

Sharpee, T. O., Sugihara, H., Kurgansky, A. V., Rebrik, S. P., Stryker, M. P., and Miller, K. D. (2006). Adaptive filtering enhances information transmission in visual cortex. *Nature*, 439(7079):936.

Skottun, B. C., Bradley, A., Sclar, G., Ohzawa, I., and Freeman, R. D. (1987). The effects of contrast on visual orientation and spatial frequency discrimination: a comparison of single cells and behavior. *J Neurophysiol*, 57(3):773–786.

Smirnakis, S. M., Berry, M. J., Warland, D. K., Bialek, W., and Meister, M. (1997). Adaptation of retinal processing to image contrast and spatial scale. *Nature*, 386(6620):69.

Snodderly, D. M. and Gur, M. (1995). Organization of striate cortex of alert, trained monkeys (macaca fascicularis): ongoing activity, stimulus selectivity, and widths of receptive field activating regions. *J Neurophysiol*, 74(5):2100–2125.

Solomon, S. G. and Kohn, A. (2014). Moving sensory adaptation beyond suppressive effects in single neurons. *Curr Biol*, 24(20):R1012–R1022.

Van Hooser, S. D., Heimel, J. A. F., Chung, S., Nelson, S. B., and Toth, L. J. (2005). Orientation selectivity without orientation maps in visual cortex of a highly visual mammal. *J Neurosci*, 25(1):19–28.

Victor, J. D. (1987). The dynamics of the cat retinal x cell centre. *The Journal of physiology*, 386(1):219–246.

Wark, B., Lundstrom, B. N., and Fairhall, A. (2007). Sensory adaptation. *Curr Opin Neurobiol*, 17(4):423–429.